Non-Faraday rotation of photon-echo polarization in ytterbium vapor

N. N. Rubtsova,* V. N. Ishchenko, E. B. Khvorostov, and S. A. Kochubei
Institute of Semiconductor Physics, Siberian Branch RAS, Acad. Lavrentyev Avenue, 13, Novosibirsk, 630090, Russia

V. A. Reshetov
Togliatti State University, Belorusskaya Street, 14, Togliatti, 445667, Russia

I. V. Yevseyev
Moscow State Engineering Physics Institute, Kashirskoye Shosse, 31, Moscow, 115409, Russia

Non-Faraday rotation of photon-echo polarization was investigated at the $J=1 \leftrightarrow J=0$ transition in a wide range of longitudinal magnetic field strength. The echo was generated at the intercombination transition $(6s6p)^3P_1 \rightarrow (6s^2)^1S_0$ of ^{174}Yb by two resonant laser pulses of linear (parallel or mutually orthogonal) polarization. A detailed analysis of the echo polarization performed by an angled echo technique has shown quite different behavior in the weak and strong magnetic field limits. The photon echo has polarization close to linear at a magnetic field strength $\mathcal{B} \lesssim 5$ G; its polarization plane rotates around the magnetic field vector clockwise or counterclockwise depending on the magnetic field orientation relative to the wave vector. The photon-echo polarization components and echo power oscillate as functions of $\mathcal{B}$. As the magnetic field increases, the oscillations become smaller and almost disappear at a magnetic field $\mathcal{B} \approx 40$ G; the photon echo does not disappear at this magnetic field, but its polarization vector no longer has a preferred orientation. Numerical calculations of the photon echo generated at a spectral wide line agree with the experimental behavior of the photon-echo polarization for an arbitrary magnetic field.

I. INTRODUCTION

The photon echo and its numerous modifications are known for their ability to store and reproduce optical information in the analog or digital form [1–3]. Modern experiments show a very powerful echo response [4]. The research presented here demonstrates the possibility of controlling the power and the polarization of the echo response by the application of a weak longitudinal magnetic field. The present growing interest in coherent transient phenomena is explained also by the ability in principle of the photon echo to reproduce a quantum state of light, in particular, a single-photon wave packet [5], which is very important for quantum computer modeling on the basis of entangled states of photon polarizations. In this respect, the investigation of photon-echo polarization has acquired a different basis, thus inspiring further research.

The photon echo (PE) is a coherent spontaneous medium response, which arises at a definite time after excitation by two or more pulses of radiation. Here we deal with the simplest case of only two pulses of unidirectional running waves of radiation resonant with only one atomic transition. The coherent response arises in this case at a time $t \approx 2\tau$ after the first exciting pulse arrival, where τ is the time delay between exciting pulses. Moreover, the type of transition $J=1 \leftrightarrow J=0$ is the simplest one for which the non-Faraday rotation of photon-echo polarization exists, and it is the transition for which the phenomenon has been predicted [6].

In the general case of an atomic (molecular) transition of arbitrary angular momenta of the upper J_a and lower J_b levels, the photon-echo polarization in the absence of a magnetic field depends on many factors. The most significant are the type of transition and the values of angular momenta involved J_a, J_b. Then the polarizations of the exciting pulses can contribute to PE polarization. The area of the exciting pulses estimated as $\theta_i \approx de_i T_i/\hbar$ (d is the matrix element of the transition dipole moment, e_i is the electric field amplitude of the ith pulse, and T_i is the pulse duration) can also influence the polarization of the coherent response. Finally, PE polarization can be modified by anisotropic depolarizing collisions.

As for the particular case of the $0 \leftrightarrow 1$ transition, the polarization properties of the photon echo have no dependence on the exciting pulse area [7]. Depolarizing collisions can also be neglected in our conditions, as follows from experimental results on PE generated by crossed linearly polarized laser pulses (see Sec. III for details). So the polarization of the PE generated at the $0 \leftrightarrow 1$ transition in the absence of a magnetic field should be determined exclusively by the level structure and by the polarization of the exciting pulses.

The physical nature of the longitudinal magnetic field effect can be understood by the following considerations. Let both wave vectors $\vec{k}_i$ of the exciting pulses be parallel to the Oz direction, as in Fig. 1. The longitudinal magnetic field is also oriented along Oz. It is natural to choose this direction as the quantization axis. For this experimental geometry, right- and left-circular waves, propagating along the Oz direction, are the eigenstates of the electromagnetic wave polarization.

*Email address: rubtsova@isp.nsc.ru
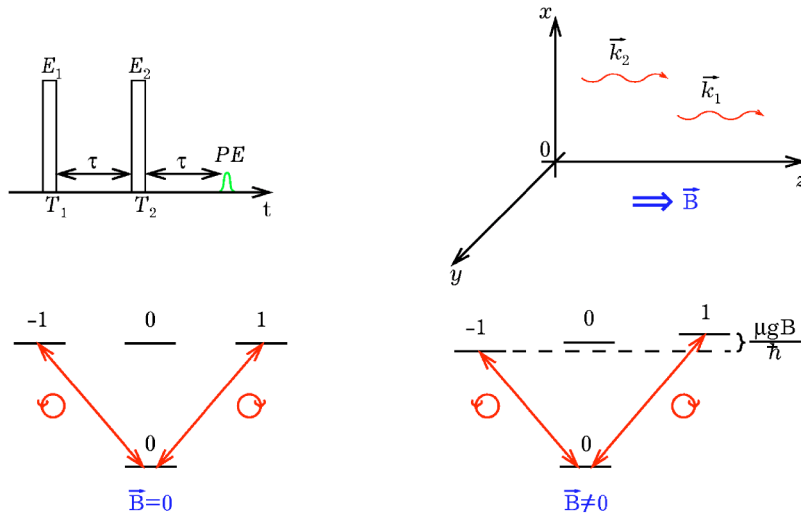
FIG. 1. Top: Temporal disposition (left graph) of a photon echo and exciting pulses of amplitude e_i and duration T_i; spatial disposition (right graph) of magnetic field $\vec{\mathcal{B}}$ and wave vectors $\vec{k}_i$. Bottom: level configuration for $0 \leftrightarrow 1$ transition in zero (left graph) and nonzero (right graph) magnetic field $\mathcal{B}$.

The upper level is triply degenerate in the absence of a magnetic field, as represented in the bottom left part of Fig. 1. The electric field vectors of the exciting pulses oscillate in the xOy plane; depending on the experimental conditions they are oriented either both parallel to the Ox axis or with the second pulse electric field parallel to the Oy axis. Exciting radiation linearly polarized along the Ox direction is equivalent to the sum of equal right- and left-circular components. These two components create optical coherences at the transitions $M=0 \leftrightarrow M=-1$ and $M=0 \leftrightarrow M=+1$ according to the selection rules. When the exciting radiation pulse stops, both coherences start oscillations at the same frequency $\omega_{ab}+kv_z$. This process is known as free polarization decay due to Doppler dephasing of the excited (within a definite range of longitudinal velocities v_z) ensemble of particles. As a result, the macroscopic polarization of the ensemble disappears, but this is not true for the microscopic polarization of each individual subclass of velocity v_z. The second pulse is able to compensate this reversible dephasing by phase conjugation. As a result, the Doppler phases $kv_z\tau$ acquired by the end of the time delay interval τ become converted to $-kv_z\tau$ after interaction with the second pulse, which allows one to restore the initial phases of an ensemble at the end of the second temporal interval τ and to create a coherent response. If the second pulse is polarized linearly like the first one, the coherent response also has the same linear polarization, generated as the sum of two identical circular components of light. The common phase factor of $e^{i\omega_{ab}\tau}$ does not contribute to the final result, i.e., to the polarization of the photon echo.

The situation changes drastically in the presence of a weak magnetic field (right bottom part of Fig. 1) because of the Zeeman splitting $\mu g \mathcal{B}/\hbar$, where μ is Bohr's magneton, g is the g factor of the upper level, and $\mathcal{B}$ is the magnetic field strength. The term "weak" means here that the Zeeman splitting is small in comparison with the spectral width of the exciting pulses $1/T_i$; therefore both transitions are excited in a symmetric manner. Now each right and left component of the microscopic polarization make free oscillations at its own frequency $\omega_{ab}-\mu g \mathcal{B}/2\hbar+kv_z$ and $\omega_{ab}+\mu g \mathcal{B}/2\hbar+kv_z$, respectively. That is why the phase difference of $\mu g \mathcal{B}\tau/\hbar$ between the right and left components of the circular polariza-

tion should be taken into account at the moment of rephasing. This results in a linear polarization of the photon echo rotated by an angle $\phi = \mu g \mathcal{B}\tau/\hbar$.

This phenomenon is known as non-Faraday rotation of PE polarization in a longitudinal magnetic field. The rotation angle does not depend on the optical density of the vapor, it depends only on the magnetic field strength, g factor, and time delay between exciting pulses. After prediction of the phenomenon for the $0 \leftrightarrow 1$ transition [6], the non-Faraday rotation was analyzed for the case of large angular momenta $J \gg 1$, small area of exciting pulses, and nearly equal g factors of the working levels [8]. A theoretical analysis for arbitrary area of the exciting pulses, arbitrary transitions, and nonequal g factors was performed in [9]. The last work can be considered as the most general one, with only one limitation of short exciting pulses $T_i \ll \tau$. According to the analytical results [9], the echo power should oscillate versus magnetic field strength for any angular momentum and for any type of spectral transition (excluding the case of the PE at the $1/2 \leftrightarrow 1/2$ transition). These PE power oscillations are largest (from maximum to zero) for the $J=1 \leftrightarrow J=0$ transition. The photon echo generated at the $J=1 \leftrightarrow J=0$ transition by two pulses with linear polarization parallel to the Ox axis has the following electric field components:

$$e_x^{PE} = \frac{1}{9}(1 + \cos 2\varepsilon_a \tau), \tag{1}$$

$$e_y^{PE} = \frac{1}{9}\sin 2\varepsilon_a \tau, \tag{2}$$

where $\varepsilon_a = \mu g_a \mathcal{B}/\hbar$, and $g_a = 1.5$ is the g factor of the upper level of the transition. The observable quantities—the echo power components of the polarization—behave according to

$$P_x^{PE} \propto (e_x^{PE})^2 \propto \cos^4 \varepsilon_a \tau, \tag{3}$$

$$P_y^{PE} \propto (e_y^{PE})^2 \propto \sin^2 2\varepsilon_a \tau. \tag{4}$$

Oscillations from maximum value to zero should be observed for both PE components and the y component should oscillate at a twice higher frequency.
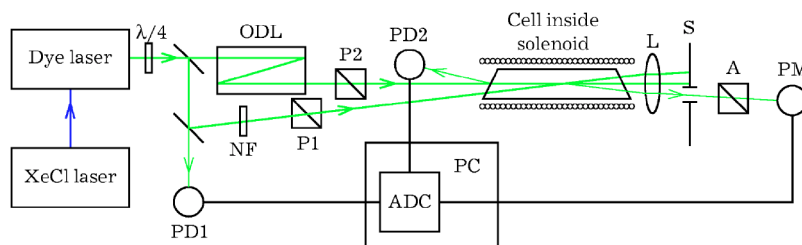
FIG. 2. Experimental arrangement: $\lambda/4$, quarter-wave plate; ODL, optical delay line; NF, neutral-density optical filter; P1,P2, Glan-Taylor prisms; PD1, photodiode for ADC triggering; PD2, photodiode for exciting pulse power control; L, lens; S, adjustable slit for spatial separation of the echo signal from exciting pulses; A, analyzer of PE polarization; PM, photoelectric multiplier; ADC, analog-to-digital converter; PC, personal computer.

Experimental research has been represented up to now by earlier results for atomic cesium vapor [10] (angular momentum of lower level $J_b = 3$ or 4 and unresolved hyperfine structure of upper level with $J_a = 3$ and 4) and molecular iodine (unidentified $J \gg 1$ angular momenta) [11]. Because of experimental difficulties in detecting the relatively weak echo signal with the background of much more powerful exciting pulses, only the PE polarization component orthogonal to the polarization of the exciting pulses was investigated in both works.

The application of the angled echo technique proved useful for the spatial separation of the echo beam from the exciting beams in our experiment [12]. This technique permitted us to study both polarization components of the photon echo and to reconstruct completely the behavior of the photon-echo polarization vector in a longitudinal magnetic field. However, a remarkable disagreement between the experimental results and a simplified theory used for their treatment was revealed there.

Here we represent a comparison of experimental data with numerical calculations that account for the final duration of the exciting pulses. These calculations provide acceptable semiquantitative agreement with the experimental data. In Sec. II of this paper we describe the experimental arrangement and the technique of data acquisition and treatment. Basic requirements for the theoretical model are also formulated. A comparison of the experimental results with numerical calculations is the subject of Sec. III. Details of the general theoretical approach and numerical calculations are placed in the Appendix. A short summary of the results, qualitative explanation of the physics, and a discussion of the reasons for the residual disagreement between theory and experiment are given in Sec. IV.

II. EXPERIMENTAL ARRANGEMENT

The experimental setup is drawn in Fig. 2. A rhodamine 110 dye laser with optical pumping by a XeCl excimer laser (308 nm wavelength, 5–6 ns pulse duration, 20 mJ average pulse energy) was used as a source of radiation at $\lambda = 555.6$ nm resonant with the intercombination transition $(6s6p)^3P_1 \rightarrow (6s^2)^1S_0$ of ^{174}Yb.

To suppress the influence of power and spatial distribution instabilities of the excimer laser on the data, several technical solutions were implemented, including special design of the dye laser and external optical scheme, investigation of the dye laser's radiation properties, and special techniques of data acquisition and treatment.

The dye laser consisted of a short (10 cm) cavity master oscillator and two sequential amplification stages. Slow circulation of the alcohol dye solution was ensured for each of these units. The master oscillator cavity was formed of a 1800 grooves/mm grating, operating in the second diffraction order in the autocollimation regime, and an output dielectric mirror. The grating was placed inside a vacuum chamber with a controllable dry nitrogen pressure, allowing fine-tuning of the master oscillator frequency. An additional 1200 grooves/mm diffraction grating placed behind the master oscillator served as a spectral selector for rejection of spontaneous emission of the dye cell.

Spatial-angular selectors, consisting of two positive lenses with a diaphragm between them, were placed between the master oscillator and the first amplification stage, as well as between the different amplification stages. The central part of the beam emerging from the final amplification stage was extracted by a 1.5 mm diameter diaphragm and expanded by a Kepler telescope up to 10 mm diameter to be delivered to the external optical scheme. The application of spatial-angular selectors and a telescopic beam expander allowed us to reduce the background related to the superluminescence of the dye and to prepare a radiation beam with a sufficiently uniform transverse intensity distribution and a divergence close to the diffraction limit.

The external optical scheme included beam splitters and a spatial optical delay line (ODL) to create a pair of coherent exciting pulses, and two Glan-Taylor prisms (P1 and P2) as independent polarizing elements for each of the two exciting pulses. A quarter-wavelength plate inserted between the output beam and beam splitter guaranteed the choice of the arbitrary polarization of each exciting pulse using the Glan-Taylor prism orientation. The film polarizer (A) placed after the working cell provided polarization analysis of the photon echo, detected by a highly sensitive short time response photomultiplier (PM). An additional photodiode (PD2) was used to control the power of both exciting pulses. All the signals were converted into digital form by an analog-to-digital converter (ADC) triggered by the first exciting pulse detected by the photodiode PD1.

The Yb vapor heated cell surrounded by a solenoid could operate in a wide temperature range. The data reported here were obtained at 800 K; metallic ytterbium of 0.999 purity and of natural isotope content was used.
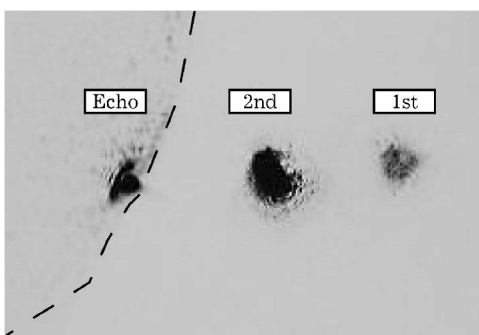
FIG. 3. Spatial distribution of the photon echo and pump pulses recorded with a web camera. Neutral optical filter with a transmission of 0.2%, attenuating the pump pulses, is located to the right of the dashed line. Photon echo is partially scattered at the edge of filter.

The angled echo technique, known since early experimental work on photon echo [13], provided here the visual observation of the photon echo. Figure 3 represents a record made by a Creative WebCam 3 web camera. However, to make actual measurements, an adjustable slit (S) was used to prevent the photomultiplier from blending the wings of the exciting pulses. An angle between the wave vectors of the exciting pulses of about 1.8×10^{-3} rad proved enough for spatial resolution of the echo beam and powerful exciting beams; meanwhile, its value was sufficiently small as to ensure negligible echo damping because of worse overlapping of the exciting beams within the cell. The estimates [12] confirming the last statement have been made for our experimental conditions according to [14].

The control of the power of the exciting pulses by the fast ADC showed fluctuations of up to 100% from pulse to pulse. Therefore the data acquisition procedure included discarding coherent responses generated by exciting pulses of power fluctuation exceeding 10%. In addition an empirical dependence of the PE signal on each of the exciting pulses' power was applied to make a correction of each echo signal according to the values of both exciting pulses measured in the same realization. The mentioned empirical dependencies have shown an increase of PE signal versus exciting pulse power up to their maximal values, thus leading us to the conclusion that exciting pulse areas were not over $\pi/2$ for the first pulse and not over π for the second one.

The data represented in the next section were acquired as a result of coherent responses averaged over 30-40 successive pulses, first treated as indicated above.

Another important feature of the experimental arrangement is the spectrum of the dye laser. Averaged over 40 laser pulses, the spectral width was measured by a 10 mm base tunable Fabry-Pérot interferometer and proved to be 3–4 GHz. This width can be considered as small enough to ensure the excitation of only even isotopic components of ytterbium, with zero nuclear spin and, hence, without hyperfine structure of the working levels. An interference picture of a single laser pulse transmitted through the Fabry-Pérot interferometer was detected by the web camera and clearly showed the multimode structure of the radiation. We can conclude on the base of this observation that each laser pulse

contained from one to four modes, this number fluctuating from pulse to pulse. The spectral separation between modes was determined by the distance between longitudinal modes of the master oscillator of 1.5 GHz, while the spectral width of each mode can be estimated from the pulse duration as $1/(2\pi T_i) \approx 30$ MHz.

It is worth emphasizing that the optical delay line provided a time delay τ between exciting pulses of 36 ns, which is comparable to the pulse duration of 5 ns. So the conventional theoretical approach $T_i \ll \tau$ convenient for obtaining analytical results is not valid, and numerical calculations are inevitable.

III. COMPARISON OF EXPERIMENTAL RESULTS AND NUMERICAL CALCULATIONS

First of all, the polarization of the photon echo generated in ytterbium vapor at the intercombination transition $(6s6p)^3P_1 \rightarrow (6s^2)^1S_0$ of ^{174}Yb by two laser pulses of identical linear polarization was investigated in a weak magnetic field $\mathcal{B} \le 5$ G. According to [8] and references cited therein, the PE should conserve linear polarization, and the polarization vector should make a clockwise precession around the magnetic field vector. For an observer looking in the $-Oz$ direction, as in our experiment, this will result in counterclockwise rotation of the photon-echo polarization plane by an angle determined by the magnetic field strength, the time delay between exciting pulses, and the spectral properties of the transition.

The polarization of the photon echo generated by two laser pulses of identical linear polarization was investigated in a weak magnetic field using an analyzer placed before the detector. The PE power dependence versus analyzer rotation angle (polarization indicatrix) is represented in Fig. 4. Each graph contains experimental points (squares) and a smooth solid line, plotted by the *B*-spline method. The two left graphs show the polarization indicatrix of the second exciting pulse. Both left figures have zero waists, proving linear polarization of the exciting pulses (it is worth emphasizing the absence of any remarkable rotation of the polarization plane of the exciting pulse for all values of the magnetic field applied in our experiment, i.e., the absence of Faraday rotation).

The right column of Fig. 4 shows the polarization indicatrices of the photon-echo responses. The waists are not exactly zero, but they are close to it. So the PE polarization is nearly linear in a weak magnetic field. In a field of 2 G the symmetry axis of the figures representing the PE polarization is rotated as compared to the exciting pulses by an angle of about 30°.

As the magnetic field changes its direction from parallel relative to the wave vector to antiparallel, the photon-echo polarization rotation changes from $-30°$ in the right top graph to $+30°$ in the right bottom graph of Fig. 4.

Further research concerned the behavior of both x and y components of the photon-echo polarization as a function of magnetic field strength. Two series of experiments were realized here—one for an echo generated by exciting pulses of parallel linear polarization (denoted below as $\uparrow\uparrow$ for brevity)
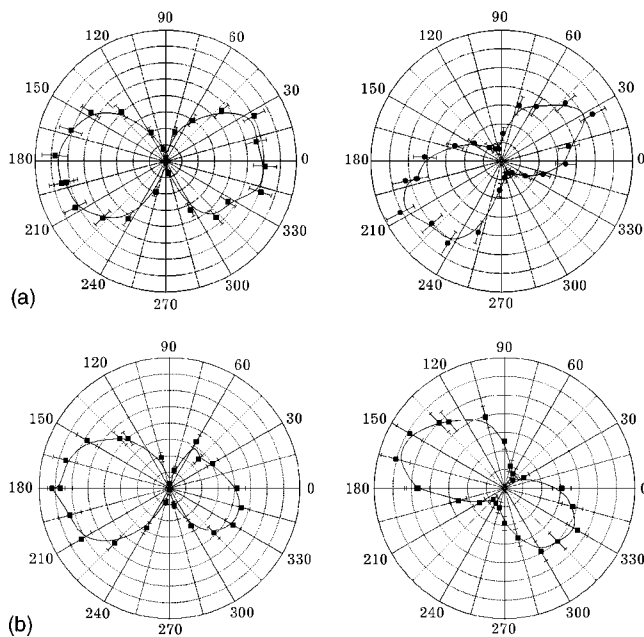
FIG. 4. Polarization indicatrices of exciting pulses (left column) and photon echoes (right column) in longitudinal magnetic field of about 2 G. Narrow waist proves that the PE polarization is close to linear. The axis of the right upper figure rotated by −30° corresponds to clockwise rotation when looking along $\vec{\mathcal{B}}\|\vec{k}$. The inverted direction of the magnetic field $\vec{\mathcal{B}}\|-\vec{k}$ results in counterclockwise rotation detected as +30°.

and the other for an echo generated by exciting pulses of mutually orthogonal (crossed) linear polarization (denoted as ↑→).

In the case of ↑↑ excitation, both the x- and y-polarization components reveal oscillations versus magnetic field strength $\mathcal{B}$, as is clear from the left column of Fig. 5. Each experimental point (black square) was obtained for a fixed value of $\mathcal{B}$ and definite position of the analyzer A as a result of 40 successive laser pulses, as described in Sec. II. The smooth solid line in each graph is the result of averaging five neighboring experimental points and is placed for convenience. Numerical calculations performed for a wide range of magnetic field strength are shown by dashed lines. In agreement with the simplified treatment according to Eqs. (1) and (2), the oscillation frequency of the y-polarization component $P_y^{\uparrow\uparrow}$ is approximately twice higher than that of the x component $P_x^{\uparrow\uparrow}$. As the magnetic field increases, the disagreement with the simplified theory becomes remarkable; the oscillation amplitudes of both x- and y-polarization components become less and the minima move away from zero.

The magnetic field dependence of the photon echo generated by exciting pulses of crossed linear polarizations ↑→ was investigated experimentally for some larger magnetic field strengths. The results are represented in the right column of Fig. 5. Neither the x nor the y photon-echo component was observed in zero magnetic field, thus confirming the negligible influence of depolarizing collisions in our experimental conditions (photon echo can be observed in ytterbium vapor for crossed linear polarizations of exciting pulses only in the presence of a considerable amount of buffer gas,

as follows from our preliminary results [15]). The echoes appear in nonzero magnetic field. Their general behavior resembles the behavior of echoes generated by pulses of parallel linear polarizations. The frequency of $P_y^{\uparrow\rightarrow}$ oscillations is approximately twice higher than the frequency of $P_x^{\uparrow\rightarrow}$ oscillations.

As the magnetic field grows, the minima of both experimental and theoretical curves move away from zero, and finally the oscillations disappear in the strong field limit, which is especially well seen in the right bottom graph of Fig. 5. The disagreement with the simplified theory, predicting oscillations between maximum and zero, proves considerable at strong magnetic fields.

The general behavior of the experimental magnetic field dependencies is well reproduced by the calculations. The discrepancies between the oscillation amplitudes of the experimental data and the theory are not surprising if we keep in mind the instabilities of the laser power and the relatively large time intervals necessary to make experiment in a wide range of the magnetic field. In addition, all the experimental curves demonstrate oscillations that look slightly accelerated relative to the corresponding theoretical curves. In this context it is worth recalling that calculations are made for exactly resonant radiation, but this is not true in a real experiment because of fluctuations of the dye laser frequency and radiation mode content. Another physical source of disagreement is the nonhomogeneity of the laser beam cross section, as is evident from Fig. 3. Taking into account all these considerations we conclude that there is at least qualitative agreement of the experimental magnetic field dependence with the numerical calculations represented by the dashed lines in Fig. 5.

On the basis of the experimental data in a weak magnetic field ($\mathcal{B}\leqslant 5$ G) the g factor of the upper working level $g=1.48\pm0.11$ is calculated, which is in agreement with the theoretical value of 1.5.

The data within the first period of PE polarization rotation have permitted us to reconstruct the possible relative values and orientations of the PE electric field vector in a weak, increasing magnetic field, as shown in Fig. 6. The triangles correspond to the values determined from experimental data (error bars are indicated at the bottom) and the dashed line is the simplified theory prediction. The PE electric field starts from a horizontal vector of maximum length at zero magnetic field for ↑↑ excitation. As the magnetic field increases, the vector rotates clockwise and draws a circle with its tip. For ↑→ excitation, the PE starts from zero, rising gradually and drawing the same circle with the vector tip as the magnetic field increases. So the experimental data obtained in the low magnetic field limit are in acceptable agreement with even the simplified theory.

The high magnetic field limit shows no oscillations of the photon-echo polarization components, but the photon-echo signal does not disappear. The polarization was checked for $\mathcal{B}\approx 40$ G for an echo generated by crossed linear polarizations of the exciting pulses. The echo power dependence on the analyzer azimuthal angle (polarization indicatrix) is presented in Fig. 7 and shows no preferred orientation of the echo polarization. This result and qualitative analysis of the phenomenon (see next section) allow us to use the notation of an unpolarized echo.
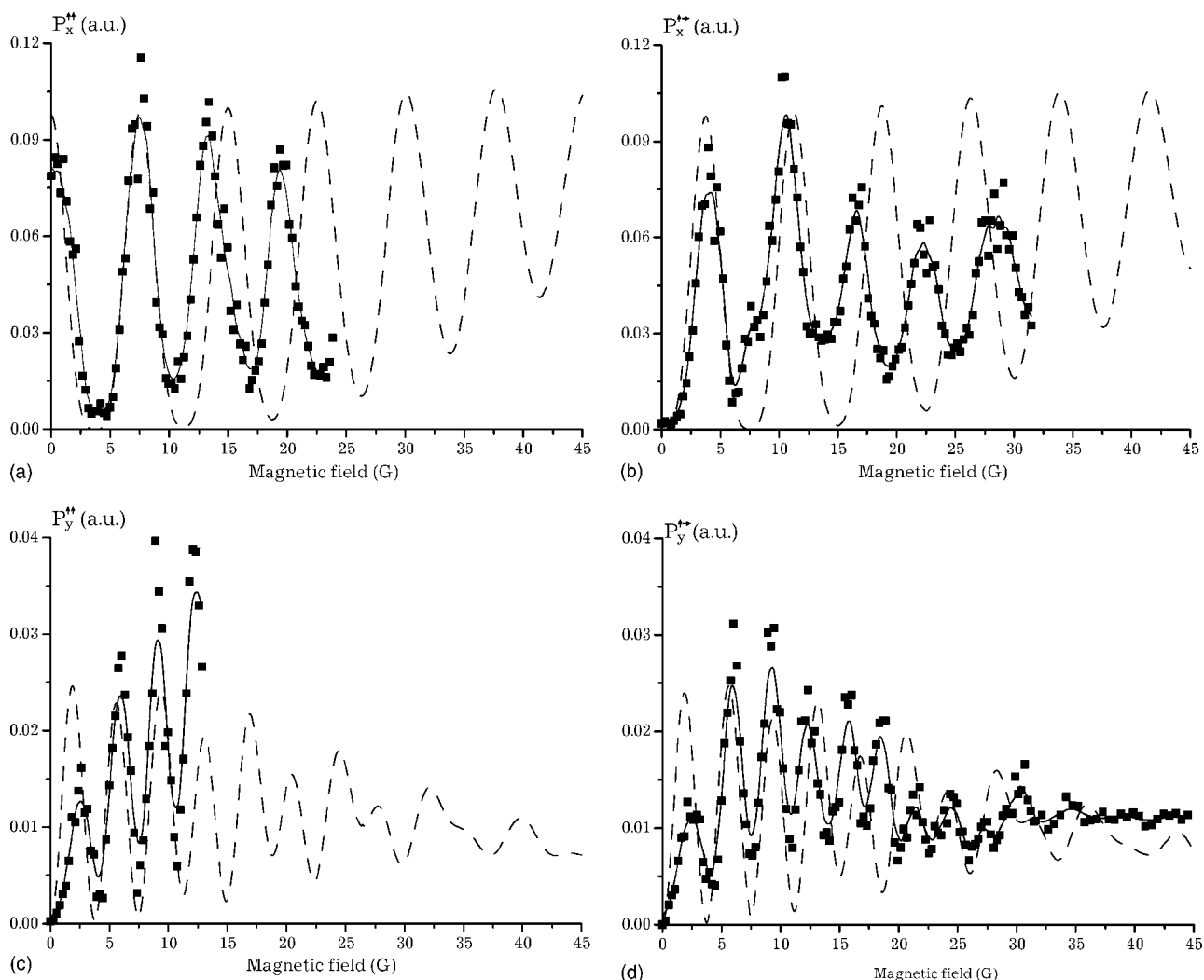
FIG. 5. Magnetic field dependence of photon echo x- (upper graph) and y- (lower graph) polarization components generated by two pulses of parallel $\uparrow\uparrow$ (left column) and crossed (right column) $\uparrow\rightarrow$ linear polarizations. Experimental points (black squares) are smoothed by solid lines; dashed lines are numerical calculations for final T_i duration. As the magnetic field grows, the minima of move away the oscillations from zero, and the oscillations become smaller and finally disappear, as is clear from both experimental results and numerical calculations.

IV. DISCUSSION

In summary, a detailed experimental and theoretical investigation of non-Faraday rotation of photon-echo polarization at the transition $0\leftrightarrow1$ in ytterbium vapor has revealed two limits of the longitudinal magnetic field where this effect looks quite different.

In the weak field limit, the situation is as follows. For the case of $\uparrow\uparrow$ excitation, the photon echo has a maximum x component and zero y component in zero magnetic field. As the magnetic field increases, the photon-echo polarization remains linear and changes its orientation; it rotates around the vector $\vec{\mathcal{B}}$ by an angle proportional to $\mu g\mathcal{B}\tau/\hbar$. This leads to oscillations of the x- and y-polarization components of the photon echo versus magnetic field strength. In the case of PE excitation by exciting pulses of crossed linear polarizations $\uparrow\rightarrow$, there is no photon echo in zero magnetic field. This experimental observation confirms that depolarizing colli-

sions are negligible in our experimental conditions. The PE polarization behavior in increasing magnetic field resembles the case of $\uparrow\uparrow$ excitation.

As follows from a simplified theoretical treatment [Eqs. (1)–(4)], both the time delay τ and the magnetic field $\mathcal{B}$ contribute in an equal manner to the rotation angle. It seemed reasonable to expect that both the time delay and the magnetic field growth should have similar effects on the PE polarization rotation, as was shown experimentally [10]. However, this is true only for the weak magnetic field limit. Increases of τ and $\mathcal{B}$ are not equivalent. Increasing τ can only improve the satisfaction of the simplified theory condition $T_i\ll\tau$, but the $\mathcal{B}$ value is an essential parameter of the problem. An increase of magnetic field strength changes the situation qualitatively; the photon echo can acquire ellipticity of polarization due to possible asymmetry of the excitation of the $M=-1$ and $M=+1$ Zeeman sublevels of the upper state. Such asymmetry could take place in our experiment because
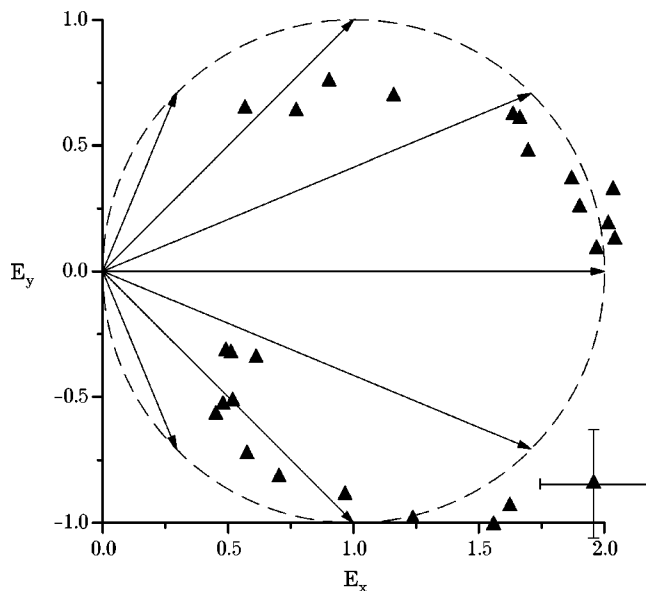
FIG. 6. Evolution of PE electric field vector in a weak magnetic field reconstructed from experimental data (triangles) and predicted by simplified theory (dashed circle).

of instabilities of dye laser radiation frequency, as was discussed in Sec. II.

In a stronger magnetic field the oscillations of the x- and y-polarization components become less and less and finally disappear. This limit of high magnetic field strength corresponds to $\mu g \mathcal{B}/\hbar \gg 1/T_i$. On one hand, this means a narrow spectral width of the exciting pulses as compared to the Zeeman splitting. On the other hand, this limit corresponds to the case when the echo duration is much longer than the
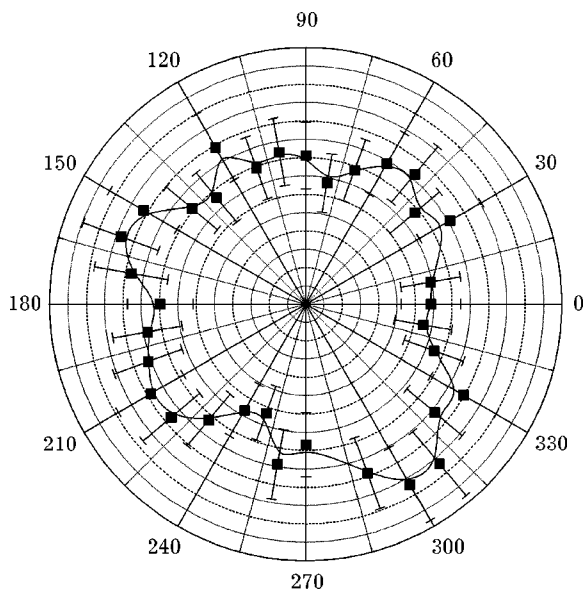
FIG. 7. Polarization indicatrix of photon echo generated at $\mathcal{B} \approx 40$ G by crossed linear polarization. It is impossible to attribute any preferred orientation to the photon-echo polarization vector within the accuracy of the experiment. The photon echo is unpolarized: it has not disappeared and no longer has a preferred orientation.

period of its polarization plane rotation. In the presence of larger frequency detuning we can probably meet the situation when only one of the Zeeman sublevels ($M=1$ or $M=-1$) of the upper level is excited, and circular echo polarization could appear. This would imply a decrease of echo power, not observed in our experiment. The case of weak frequency detuning leads to nonequal excitation of the $M=1$ and $M=-1$ Zeeman sublevels, thus leading to an elliptically polarized echo with its longer axis rotating around the magnetic field vector, while the rotation frequency is too high to make several rotations during the echo pulse. The fluctuations of frequency detuning in our experiment give us no chance to observe this transition from a linearly to an elliptically polarized echo. However, if the laser radiation had much better stability, the case of exact resonance should produce a linearly polarized echo with its polarization plane rotating around the magnetic field, and this rotation speed would be high enough to make several turns during an echo pulse. So, taking into account this consideration, we have to conclude that the photon echo detected in the high magnetic field limit is really unpolarized.

The experimentally revealed peculiarities of the photon-echo polarization behavior in a longitudinal magnetic field can also be explained qualitatively by analysis of Eqs. (A23) and (A24) of the Appendix in the limits of weak and strong magnetic fields. As discussed in the Introduction, the characteristics of the PE, its amplitude and polarization, are determined by the relative phase shifts of the various Zeeman transitions at the instant t' of rephasing, which are expressed through the exponential factors in Eqs. (A17) and (A18). Such relative phase shifts are proportional to $\mu g \mathcal{B}(\tau+t')/\hbar$, where τ is the time interval between excitation pulses. In the case of a weak magnetic field, the effect of this field may be neglected during the action of the excitation pulses and, in the course of the PE pulse duration, the instant of rephasing $t'=2\tau$ is unique for the whole of the PE pulse. In this case the PE pulse may be considered as linearly polarized, while the oscillations of its amplitude versus the magnetic field strength $\mathcal{B}$ appear to be harmonic with the only frequency $2\mu g \tau/\hbar$. This qualitative behavior is confirmed by Eq. (A23). In the case of the transitions $J_a=1 \rightarrow J_b=0$ the integrand in this formula is

$$\left| \sum_{m,\nu} G_{m\nu} \right|^2 = \left| G_- \exp\left\{ -i \frac{2\mu g \mathcal{B} \tau}{\hbar} \right\} + G_+ \exp\left\{ i \frac{2\mu g \mathcal{B} \tau}{\hbar} \right\} \right|^2,$$

where G_- and G_+ do not depend on the magnetic field strength $\mathcal{B}$. Here the exponential factors are responsible for the PE polarization rotation and for the oscillations of its amplitude versus $\mathcal{B}$. In the case of a strong magnetic field, the relative phase shifts $\mu g \mathcal{B}(\tau+t')/\hbar$ of the various Zeeman transitions occur not only in the time interval τ between the excitation pulses, but also during the action of the excitation pulses and in the course of the PE pulse duration. In this case the instants t' of rephasing cannot be considered approximately equal for all the parts of the PE pulse, but they are in the interval $(\tau-T_e/2)<t'<(\tau+T_e/2)$, where T_e is the duration of the PE pulse. If the magnetic field is strong enough, so that $\mu g \mathcal{B} T_e/\hbar > 2\pi$, then the PE polarization rotates in the

course of its duration over an angle of the order of 2π. So in this case the PE pulse is expected to be totally unpolarized. The oscillations of the PE amplitude versus the magnetic field strength in this case appear to be not pure harmonic, but a superposition of harmonic oscillations with different frequencies $\mu g(\tau+t')/\hbar$. Such a superposition leads to the detachment of the PE amplitude minimum from zero. With strong magnetic fields the integration over t' becomes an integration over an infinite region, which provides the Dirac δ function

$$\int_{-\infty}^{\infty} \exp\left\{i\frac{\mu g \mathcal{B} t'}{\hbar}\right\} dt' = 2\pi\delta\left(\frac{\mu g \mathcal{B}}{\hbar}\right),$$

so that the PE characteristics in this limit become independent of the magnetic field strength $\mathcal{B}$. This integration, which is in fact a Fourier transform, is carried out in the formula Eq. (A19). In the limit of strong magnetic field this formula is transformed to Eq. (A24). In the integrand of this latter formula $|\Sigma_{m,\nu}G_{m\nu}|^2=|G_-|^2+|G_+|^2$ the phase factors $\exp\{i2\mu g \mathcal{B}\tau/\hbar\}$, which are responsible for the dependence of the PE characteristics on magnetic field strength $\mathcal{B}$, disappear.

We attribute residual discrepancies between the experimental data and the calculations to the inaccuracy of measurements implied by the inhomogeneity of the laser beam and especially by the fluctuations of the laser frequency and mode content, which are difficult to take into account by calculations. No doubt our experimental results could be more impressive in the case of using a cw dye laser, as has been done in research on collisions by the photon-echo technique [16–18]. Further development of our experiment supposes the substitution of the pulsed master oscillator of the dye laser by a one-mode narrow line cw dye laser. However, even by using the relatively bad radiation source described above, there is the possibility of controlling the polarization and power of the photon echo by an external magnetic field. Our investigation has confirmed the possibility of rotating the polarization of the photon echo by 90% using a weak longitudinal magnetic field and even of "switching out" the photon echo.

In conclusion, non-Faraday rotation of photon-echo polarization was investigated at the $J=1\leftrightarrow J=0$ transition in a wide range of longitudinal magnetic field. The weak field limit of the magnetic field implies rotation of the PE linear polarization around the magnetic field vector clockwise or counterclockwise. The strong field limit leads to an unpolarized echo. All the experimentally revealed peculiarities of PE polarization behavior in a longitudinal magnetic field were reproduced by numerical calculations on the basis of a model of photon echo generated at a spectral wide line, valid for any magnetic field strength.

APPENDIX

The resonant degenerate atomic levels E_b and E_a [$\omega_0 = (E_b - E_a)/\hbar$] are split in a static magnetic field into a set of Zeeman sublevels

$$E_{bm} = E_b + m\epsilon_b, E_{a\mu} = E_a + \mu\epsilon_a, \tag{A1}$$

where m and μ are the projections of the total angular momenta J_b and J_a of the levels onto the quantization axis Z, which is chosen in the direction of propagation of the excitation pulses, while

$$\epsilon_b = \frac{g_b \mu_B \mathcal{B}}{\hbar}, \quad \epsilon_a = \frac{g_a \mu_B \mathcal{B}}{\hbar}, \tag{A2}$$

g_b and g_a are the g factors of the levels, μ_B is the Bohr magneton, and $\mathcal{B}$ is the magnetic field strength.

The interaction between the gaseous medium and excitation laser pulses of electric field strength

$$\vec{E}_n = \vec{e}_n \exp\{-i(\omega t - kz)\} + \text{c.c.}, \ n = 1,2, \tag{A3}$$

where $\vec{e}_n$ is the slowly varying amplitude, is described by the quantum mechanical equation

$$\left(\frac{\partial}{\partial t} + \vec{v}\,\nabla\right)\hat{\sigma} = \frac{i}{\hbar}[\hat{\sigma},\hat{H}_0 - \hat{\vec{d}}\vec{E}_n] \tag{A4}$$

for the atomic (molecular) density matrix $\hat{\sigma}$, where $\vec{v}$ is the velocity of the atom (molecule), $\hat{H}_0$ is the free atom Hamiltonian, and $\hat{\vec{d}}$, is its electric dipole moment operator.

In the rotating wave approximation we obtain the equation

$$\dot{\hat{\rho}} = i[\hat{\rho},\hat{V}] \tag{A5}$$

for the slowly varying matrix $\hat{\rho}$, whose components are defined by the relations

$$\sigma_{mm'}^{bb} = \rho_{mm'}^{bb}, \ \sigma_{\mu\mu'}^{aa} = \rho_{\mu\mu'}^{aa}, \ \sigma_{\mu m}^{ab} = \rho_{\mu m}^{ab}\exp\{-i(\omega t - kz)\}, \tag{A6}$$

while $\hat{V}$ is a square $2(J_b+J_a+1)\times 2(J_b+J_a+1)$ matrix with the following components:

$$(V_n)_{mm'}^{bb} = \delta_{mm'}\left(m\epsilon_b + \frac{\delta}{2}\right), \ (V_n)_{\mu\mu'}^{aa} = \delta_{\mu\mu'}\left(\mu\epsilon_a - \frac{\delta}{2}\right),$$

$$\delta = kv + \omega_0 - \omega,$$

$$(V_n)_{m\mu}^{ba} = ((V_n)_{\mu m}^{ab})* = -\frac{1}{\hbar}(\vec{d}\vec{e}_n)_{m\mu}^{ba}$$

$$= \frac{de_n}{\hbar\sqrt{2}}(-1)^{J_b-m}\sum_q \begin{pmatrix} J_b & 1 & J_a \\ -m & q & \mu \end{pmatrix}$$

$$\times[\delta_{q,1}\exp(-i\psi_n) - \delta_{q,-1}\exp(i\psi_n)], \tag{A7}$$

where v is the projection of the atomic velocity on the axis Oz, d is the reduced matrix element of the electric dipole moment operator of an atom for the transition $J_b \rightarrow J_a$, the $3j$ symbols are defined in the usual way, and ψ_n is the angle between the polarization vector of the nth excitation pulse and the axis Ox.

Henceforth we shall consider linearly polarized excitation pulses with constant amplitude e_n and duration T_n ($n = 1, 2$). In this case the solution of Eq. (A5) may be written in the following way:

$$\hat{\rho}_n = \hat{S}_n \hat{\rho}_{n-1} \hat{S}_n^+, \tag{A8}$$

where $\hat{\rho}_{n-1}$ and $\hat{\rho}_n$ are the atomic density matrices before the incidence and after the passage of the nth excitation pulse, while

$$\hat{S}_n = \exp(-iT_n \hat{V}_n). \tag{A9}$$

The initial atomic density matrix $\hat{\rho}_0$ at the instant of time before the incidence of the first excitation pulse is as follows:

$$\hat{\rho}_0 = n_0 f(v) |J_a, \mu\rangle\langle J_a, \mu|, \tag{A10}$$

where n_0 is the concentration of resonant atoms,

$$f(v) = \frac{1}{\sqrt{\pi} u} \exp\left(-\frac{v^2}{u^2}\right) \tag{A11}$$

is the Maxwellian distribution function, and u is the average thermal velocity of the atoms.

The electric field strength

$$\vec{E}^e(t') = \vec{e}^e(t') \exp\{-i(\omega t - kz)\} + \text{c.c.},$$

$$t' = t - z/c - T_1 - T_2 - 2\tau, \tag{A12}$$

of the photon echo formed by excitation pulses separated by the time interval τ can be obtained from the Maxwell equation

$$\left(\Delta - \frac{1}{c^2} \frac{\partial^2}{\partial t^2}\right)\vec{E}^e = \frac{4\pi}{c^2} \frac{\partial^2}{\partial t^2} Sp(\hat{\sigma}, \hat{\vec{d}}). \tag{A13}$$

The projection of its slowly varying amplitude $\vec{e}^e(t')$ on the direction of the polarizer axis

$$\vec{l} = \vec{l}_x \cos\phi + \vec{l}_y \sin\phi \tag{A14}$$

constituting an angle ϕ with the axis Ox is as follows:

$$e^e(t') = (\vec{e}^e, \vec{l}) = i \frac{e_0}{\sqrt{\pi}} \int_{-\infty}^{\infty} \exp(-x^2 - ikut'x) F(x) dx, \tag{A15}$$

$$e_0 = 2\pi\omega \frac{L}{c} n_0 |d| \exp(-2\gamma\tau), \tag{A16}$$

$$F(x) = \sum_{m, \mu} G_{m\mu}(x) \exp\{-it'(m\epsilon_b - \mu\epsilon_a)\}, \tag{A17}$$

$$G_{m\mu}(x) = \sum_{m', \mu', \mu''} \exp\{i\tau[\epsilon_b(m' - m) - \epsilon_a(\mu' - \mu)]\}$$
$$\times (\vec{g}, \vec{l})_{\mu m}^{ab} (\hat{S}_2)_{m\mu'}^{ba} (\hat{S}_2^+)_{m', \mu}^{ba} (\hat{S}_1)_{\mu', \mu''}^{aa} (\hat{S}_1^+)_{\mu'', m'}^{ab}. \tag{A18}$$

Here L is the length of the gaseous medium, $1/\gamma$ is the time of the irreversible relaxation, which is considered to be much greater than the durations of the excitation and echo pulses, $\hat{\vec{g}} = \hat{\vec{d}}/|d|$, and the matrices $\hat{S}_n$ are defined by Eq. (A9).

In the experiments the integrated intensity of the echo pulse passing through the polarizer is registered, which (in relative units) is as follows:

$$I^e = \frac{ku}{2e_0^2} \int_{-\infty}^{\infty} |e^e(t')|^2 dt'$$

$$= \sum_{m, \mu, m_1, \mu_1} \int_{-\infty}^{\infty} dx \exp\{-x^2 - (x - \xi_{m\mu m_1 \mu_1})^2\}$$

$$\times G_{m\mu}(x) G_{m_1 \mu_1}^*(x - \xi_{m\mu m_1 \mu_1}), \tag{A19}$$

where

$$\xi_{m\mu m_1 \mu_1} = \frac{1}{ku}\{\epsilon_b(m - m_1) - \epsilon_a(\mu - \mu_1)\}. \tag{A20}$$

The matrix elements of the matrices $\hat{S}_n$ in Eq. (A18) may be calculated in the diagonal representation of the matrix $\hat{W}_n = T_n \hat{V}_n$. Let us enumerate the vectors $|J_b, m\rangle$ and $|J_a, \mu\rangle$ of the initial basis by the index ν, which generally gives $2(J_b + J_a + 1)$ values so that $|\nu = 0\rangle = |J_b, m = J_b\rangle$, …, $|\nu = 2J_b\rangle = |J_b, m = -J_b\rangle$, $|\nu = 2J_b + 1\rangle = |J_a, \mu = J_a\rangle$, …, $|\nu = 2J_b + 2J_a + 1\rangle = |J_a, \mu = -J_a\rangle$.

Then

$$\langle \nu|\hat{S}_n|\nu'\rangle = \sum_j c_{j\nu}^{(n)}(c_{j\nu'}^{(n)}) * \exp(-i\lambda_j^{(n)}), \tag{A21}$$

where $\lambda_j^{(n)}$ are the eigenvalues of the matrix $\hat{W}_n$ and

$$c_{j\nu}^{(n)} = \langle \nu|u_j^{(n)}\rangle, \tag{A22}$$

while $|u_j^{(n)}\rangle$ are the corresponding eigenvectors.

In the case of a weak magnetic field ($|\epsilon_b - \epsilon_a| \ll ku$)

$$I^e = \int_{-\infty}^{\infty} dx \exp(-2x^2) \left|\sum_{m, \mu} G_{m\mu}(x)\right|^2, \tag{A23}$$

and in the case of a strong magnetic field ($\epsilon_b, \epsilon_a \gg ku$)

$$I^e = \int_{-\infty}^{\infty} dx \exp(-2x^2) \sum_{m, \mu} |G_{m\mu}(x)|^2. \tag{A24}$$

If the spectral line on which the echo is formed is narrow ($kuT_n \ll 1$), then $G_{m\mu}(x) = G_{m\mu}(0) = G_{m\mu}$ and

$$I^e = \sqrt{\frac{\pi}{2}} \sum_{m,\mu,m_1,\mu_1} G_{m\mu} G^*_{m_1\mu_1} \exp\left(-\frac{1}{2}\xi^2_{m\mu m_1\mu_1}\right),$$

$$(A25)$$

where $\xi_{m\mu m_1\mu_1}$ is defined by Eq. (A20).

The numerical calculations of the integrated intensity I^e of the echo were carried out in the exact resonance approximation for the transition with angular momenta $J_a = 1 \leftrightarrow J_b = 0$, for a broad spectral line ($ku = 3.1 \times 10^9$ s^{-1}, corresponding to Yb vapor temperature $T = 800$ K), for square excitation pulses with equal durations $T_1 = T_2 = 5.3$ ns and optimal areas $\theta_1 = \pi/2$, $\theta_2 = \pi$, ($\theta_n = 2|d|e_n T_n/\hbar\sqrt{3}$), separated by the time interval $\tau = 36$ ns. Direct matrix calculations for Eq. (A18) and integration over Eq. (A19) were made with the help of MATHCAD 8.01. Numerical plots are shown by dashed lines in Fig. 5. To facilitate the comparison between numerical and experimental data the latter were properly normalized. All peculiarities of the PE polarization component behavior versus magnetic field, including in the strong field limit, are qualitatively reproduced by the numerical calculations.

[1] N. Carlson, L. Rothberg, A. Yodh, W. Babbitt, and T. Mossberg, Opt. Lett. **8**, 483 (1983).

[2] I. Yevseyev, V. Yermachenko, and V. Samartsev, *Depolarizing Collisions in Nonlinear Electrodynamics* (Taylor & Francis, New York, 2004).

[3] V. Samartsev and S. Akhmanov, *Novel Physical Principles of Information Treatment* (Science, Moscow, 1990) (in Russian).

[4] T. Wang, C. Greinem, J. R. Bochinski, and T. Mossberg, Phys. Rev. A **60**, R757 (1999).

[5] S. Moiseev and S. Kröll, Phys. Rev. Lett. **87**, 173601 (2001).

[6] A. Alekseyev, Zh. Eksp. Teor. Fiz. Pis'ma Red. **9**, 472 (1969).

[7] A. Yevseyev, I. Yevseyev, and V. Yermachenko, Opt. Spektrosk. **50**, 77 (1981).

[8] I. Yevseyev and V. Yermachenko, Opt. Spektrosk. **47**, 1139 (1979).

[9] I. Yevseyev and V. Reshetov, Opt. Spektrosk. **57**, 869 (1984).

[10] T. Baer and I. Abella, Phys. Rev. A **16**, 2093 (1977).

[11] I. Popov, I. Bikbov, I. Yevseyev, and V. Samartsev, Zh. Prikl. Spektrosk. **52**, 794 (1990).

[12] V. Ishchenko, S. Kochubei, N. Rubtsova, E. Khvorostov, and I. Yevseyev, Laser Phys. **12**, 1079 (2002).

[13] N. Kurnit, I. Abella, and S. Hartmann, Phys. Rev. Lett. **13**, 567 (1964).

[14] R. Beach, B. Brody, and S. Hartmann, Phys. Rev. A **27**, 2925 (1983).

[15] V. Ishchenko, S. Kochubei, N. Rubtsova, E. Khvorostov, and I. Yevseyev (unpublished).

[16] A. Ghosh, C. Nabors, M. Attili, and J. Thomas, Phys. Rev. Lett. **54**, 1794 (1985).

[17] J. Thomas, A. Ghosh, and M. Attili, Phys. Rev. A **33**, 3029 (1986).

[18] J. Liang, R. Dasari, M. Feld, and J. Thomas, J. Opt. Soc. Am. B **3**, 506 (1986).